

Single-particle spectral function of quarter-filled ladder systems

M. Aichhorn, E. Ya. Sherman, and H. G. Evertz

Institut für Theoretische Physik, Technische Universität Graz, Petersgasse 16, A-8010 Graz, Austria

We study the single-particle properties of quarter-filled ladder systems such as α' -NaV₂O₅ by means of a recently developed generalization of the variational cluster perturbation theory to extended Hubbard models. We find a homogeneous antiferromagnetic insulating phase for nearest-neighbor repulsions smaller than a critical value, without any metallic phase for small repulsions. Different from C-DMFT and LDA considerations, the inclusion of diagonal hopping within a ladder has little effect on the bonding bands, while flattening and shifting the antibonding bands. In the low-temperature charge-ordered phase, the spectrum depends on whether the ordering is driven by the Coulomb repulsion or by the coupling to a static lattice distortion. The small change of the experimentally observed gap upon charge ordering implies that the lattice coupling plays an important role in this ordering. Inter-ladder coupling is straightforward to include within our method. We show that it has only a minor effect on the spectral function. The numerically calculated spectra show good agreement with experimental angle-resolved photo-emission data.

PACS numbers: 71.10.Fd, 71.38.-k

I. INTRODUCTION

In recent years low-dimensional strongly-correlated systems have been the subject of many experimental and theoretical studies due to their fascinating properties such as the occurrence of ordered patterns of the ion charges. A compound in this class of materials is the low-dimensional vanadium bronze α' -NaV₂O₅. Although known for many years¹ it has attracted considerable attention in recent years because of a very interesting low-temperature phase. The compound exhibits a spin-Peierls-like transition at $T_c \approx 35$ K accompanied by the opening of a spin gap.² At the same³ or slightly higher temperature charge ordering takes place. Different from the first X-ray investigations, recent studies^{4,5,6} at room temperature showed a disordered state with equivalent valence 4.5 for all vanadium ions. Below the phase transition point, NMR-studies⁷ gave two different valences for the ions, a clear evidence for the formation of a charge-order pattern below T_c . Since one d_{xy} electron is shared by two V sites in a V-O-V rung, the ordering occurs as a static charge disproportion δ between the V ions, yielding charges $4.5 \pm \delta$ with a zig-zag pattern of δ 's. Since the crystal environment of the vanadium ions is asymmetric, the d_{xy} electrons are coupled to the lattice via a strong Holstein-like electron-phonon interaction.⁸ This results in a static lattice distortion below the charge ordering transition temperature, where the ion displacements from their positions in the high-temperature phase is of the order of 0.05 Å as observed in X-ray diffraction experiments.⁹

Although the crystal structure of α' -NaV₂O₅ is composed of nearly decoupled two-dimensional layers that consist of coupled two-leg ladders, spin-susceptibility measurements² revealed that the system can be reasonably well described by a one-dimensional Heisenberg model. This behavior could be explained by realizing that the molecular-orbital state on a rung occupied by one electron is a key element of the electronic

structure,¹⁰ yielding quasi 1D magnetic exchange couplings. In addition angle-resolved photo-emission spectroscopy (ARPES), performed in the disordered high-temperature phase showed quasi 1D band dispersions of the vanadium 3d bands,^{11,12} and it was argued that spin-charge separation should be present in this system.¹³

Previous studies^{14,15,16,17} revealed that the electron-phonon coupling is very important for the phase transition in quarter-filled ladder compounds. For this reason we study a model Hamiltonian that includes the coupling of the d_{xy} electrons to the lattice. The relevant parameters for the study of lattice effects can be obtained from experiments¹⁸ (phonon frequencies), and from first-principle calculations (lattice force constants and electron-phonon coupling).^{5,19}

Static and dynamic properties of quarter-filled ladder compounds without coupling to the lattice have been studied intensively in the past using different methods like mean-field approaches,^{20,21,22} exact diagonalisation (ED) of small clusters,^{23,24,25,26} density-matrix renormalization-group (DMRG),²⁷ cluster dynamical mean-field theory (C-DMFT),²⁸ and bosonization and renormalization-group techniques.²⁹ Recently the influence of the lattice coupling on the charge-ordering transition was investigated by employing ED methods.¹⁷

In this paper we study the single-particle spectral function of the compound α' -NaV₂O₅, which can be directly related to the ARPES experiments, by applying the recently proposed variational cluster perturbation theory (V-CPT).³⁰ This method is a combination of the cluster perturbation theory³¹ and the self-energy functional approach (SFA),³² which provides results for the infinite lattice and allows to study symmetry-broken phases. It was used with success for the investigation of the magnetic ground-state properties of the two-dimensional Hubbard model.³³ For Hamiltonians including offsite Coulomb interactions an extension of this theory has been developed,³⁴ which turned out to give very accu-

rate results for the one and two-dimensional extended Hubbard model.

The paper is organized as follows. In Sec. II we introduce the model Hamiltonian and give a short description of the V-CPT method. Sec. III and Sec. IV includes our results for single and coupled ladders, respectively, and we finally draw our conclusions in Sec. V.

II. MODEL AND METHOD

On a microscopic level α' -NaV₂O₅ can be described by an extended Hubbard model (EHM). In order to take into account lattice effects we further extend this well-known model by electron-phonon coupling terms, yielding the model

$$H = H_{\text{EHM}} + H_{\text{l}} + H_{\text{e-l}}, \quad (1)$$

with H_{EHM} the EHM Hamiltonian, H_{l} the contribution of the lattice, and $H_{\text{e-l}}$ a Holstein-like electron-phonon coupling. These terms are given by

$$H_{\text{EHM}} = - \sum_{\langle ij \rangle, \sigma} t_{ij} (c_{i\sigma}^\dagger c_{j\sigma} + \text{H.c.}) + U \sum_i n_{i\uparrow} n_{i\downarrow} + \sum_{\langle ij \rangle} V_{ij} n_i n_j, \quad (2a)$$

$$H_{\text{l}} = \kappa \sum_i \frac{z_i^2}{2}, \quad (2b)$$

$$H_{\text{e-l}} = -C \sum_i z_i n_i, \quad (2c)$$

where $\langle ij \rangle$ connects nearest-neighbor bonds, and t_{ij} is the corresponding hopping matrix element. In Fig. 1 the lattice structure and the hopping processes used in this study are shown. The most commonly used set for these matrix elements is $t_a = 0.38$ eV, $t_b = 0.18$ eV, and $t_{xy} = 0.012$ eV, and was obtained by fitting the LDA bands.⁵ A recent study¹⁹ gave similar parameter values. By including the additional hopping term t_d in a massive downfolding procedure, Mazurenko *et. al.*²⁸ found similar values for t_a and t_{xy} , but the values $t_b = 0.084$ and $t_d = 0.083$ differ considerably from previous studies. In this study we set t_a as the energy unit and fix $t_b = 0.5$, except for Sec. III C, where we study the spectral function including the hopping term t_d . The onsite Coulomb interaction is set to $U = 8$ throughout the paper, in accordance with band-structure calculations,¹⁹ and the inter-site Coulomb interaction V_{ij} is treated as a free parameter of the system, since the determination of a proper value within first-principle calculations is very difficult.

The lattice distortions are given in units of 0.05 Å, since the ion displacements in the ordered phase are of this order of magnitude. The electron-phonon coupling C and the lattice rigidity κ were determined by first-principle calculations¹⁹ yielding $C = 0.35$ and $\kappa = 0.125$ within

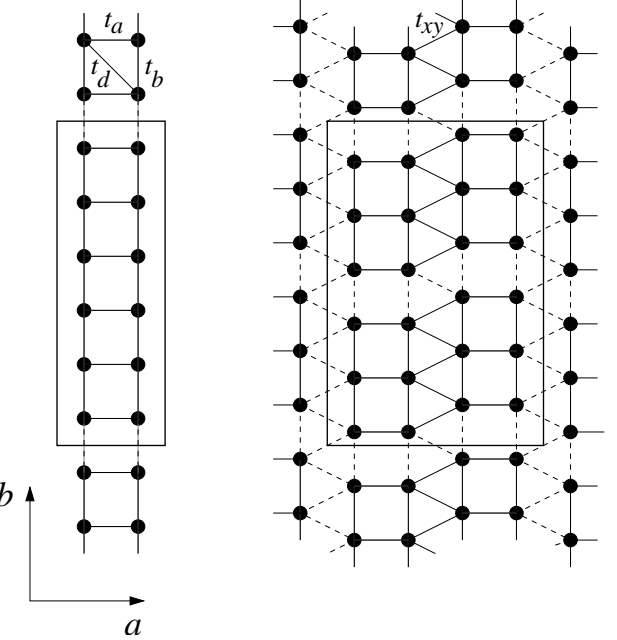


FIG. 1: Clusters used for the V-CPT calculations. The diagonal hopping t_d is indicated only once, but is present equivalently between other sites. Decoupled bonds treated perturbatively are marked by dashed lines, and the boxes show the clusters of finite size. Left: Single ladder with 6×2 cluster. Right: Super cluster consisting of two 12 site clusters.

these units. We restrict our investigations to static distortions and neglect dynamical phonon effects, similar to parts of Ref. 17.

The method we use in this paper for the calculation of the single-particle spectrum is the variational cluster perturbation theory for an EHM.³⁴ The main idea is to decouple the lattice into clusters of finite size as depicted in Fig. 1, yielding the Hamiltonian

$$H = \sum_{\mathbf{R}} \left[H_0^{(\text{c})}(\mathbf{R}) + H_1(\mathbf{R}) \right] + \sum_{\mathbf{R}, \mathbf{R}'} H_0^{(\text{i})}(\mathbf{R}, \mathbf{R}'), \quad (3)$$

where \mathbf{R} denotes the individual clusters. The first sum consists of decoupled intra-cluster Hamiltonians with interaction part $H_1(\mathbf{R})$, and the second sum gives the coupling between clusters, which must be of single-particle type and is of the general form

$$H_0^{(\text{i})}(\mathbf{R}, \mathbf{R}') = \sum_{a,b} T_{a,b}^{\mathbf{R}, \mathbf{R}'} c_{\mathbf{R}, a}^\dagger c_{\mathbf{R}', b}. \quad (4)$$

The indices a and b are orbital indices within a cluster. Obviously the Hamiltonian (3) is invariant under the transformation

$$\begin{aligned} H_0^{(\text{c})}(\mathbf{R}) &\rightarrow H_0^{(\text{c})}(\mathbf{R}) + \mathcal{O}(\mathbf{R}) \\ H_0^{(\text{i})}(\mathbf{R}, \mathbf{R}') &\rightarrow H_0^{(\text{i})}(\mathbf{R}, \mathbf{R}') - \delta_{\mathbf{R}, \mathbf{R}'} \mathcal{O}(\mathbf{R}), \end{aligned} \quad (5)$$

with an arbitrary single-particle operator

$$\mathcal{O}(\mathbf{R}) = \sum_{a,b} \Delta_{a,b} c_{\mathbf{R},a}^\dagger c_{\mathbf{R},b}. \quad (6)$$

This transformation allows the study of symmetry-broken phases by the inclusion of fictitious symmetry-breaking fields. In the present case of the EHM the intercluster Coulomb interactions are decoupled on a mean-field level, giving effective onsite potentials λ_i on the cluster boundaries.³⁴ The interactions within the individual clusters are treated exactly by the Lanczos method.

The proper values of these mean-field potentials as well as the proper choice of the single-particle operator $\mathcal{O}(\mathbf{R})$ are determined within the framework of the SFA. It provides a unique way to calculate the grand potential of a system by using dynamical information of an exactly solvable reference system, which is in our case the decoupled cluster. This grand potential is parametrized as a function of the matrix of single-particle parameters $\Delta = \Delta_{a,b}$ for the operator (6) and the mean-field parameters λ_i , and the functional form is taken from Refs. 32,34:

$$\begin{aligned} \Omega(\Delta, \lambda_i) = \Omega'(\Delta, \lambda_i) \\ + T \sum_{\omega_n, \mathbf{q}} \text{tr} \ln \frac{-1}{\mathbf{G}_q^{(0)}(\lambda_i, i\omega_n)^{-1} - \Sigma(\Delta, \lambda_i, i\omega_n)} \\ - LT \sum_{\omega_n} \text{tr} \ln(-\mathbf{G}'(\Delta, \lambda_i, i\omega_n)), \end{aligned} \quad (7)$$

where $\Omega'(\Delta, \lambda_i)$ is the grand potential of the decoupled clusters, $\mathbf{G}_q^{(0)}(\lambda_i, i\omega_n)$ is the non-interacting Green's function of the original infinite-lattice problem after mean-field decoupling of inter-cluster Coulomb interactions, $\Sigma(\Delta, \lambda_i, i\omega_n)$ is the cluster self energy, $\mathbf{G}'(\Delta, \lambda_i, i\omega_n)$ the cluster Green's function and L denotes the number of clusters. All cluster properties can easily be calculated by the Lanczos algorithm. The sum over Matsubara frequencies in Eq. (7) is evaluated by a continuation to the real frequency axis, $i\omega_n \rightarrow \omega + i0^+$, yielding an integral from minus infinity to μ (note that the Hamiltonian, Eq. (1), does not involve μ in any way). The physical grand potential is given by the stationary point of $\Omega(\Delta, \lambda_i)$, and the single-particle Green's function is then calculated by

$$\mathbf{G}_q(\omega) = [\mathbf{G}'(\omega)^{-1} - \mathbf{T}_q]^{-1} \quad (8)$$

with the Fourier-transformed matrix elements $T_{q,a,b}$.³¹ After applying a residual Fourier transformation³¹ one finally obtains the fully momentum-dependent Green's function $G(\mathbf{k}, \omega)$ for the infinite size system.

Since calculations are not done at half filling, the chemical potential is not known a priori. However, the knowledge of μ is important for the evaluation of the grand potential, as discussed above. For this purpose one can calculate μ from the condition

$$n = \frac{2}{L} \sum_{\mathbf{k}} \int_{-\infty}^{\mu} d\omega A(\mathbf{k}, \omega), \quad (9)$$

where the spectral function $A(\mathbf{k}, \omega)$ is given by

$$A(\mathbf{k}, \omega) = -\frac{1}{\pi} \text{Im} G(\mathbf{k}, \omega + i\eta) \quad (10)$$

and η is a small Lorentzian broadening. This looks like a self-consistent procedure, since for the calculation of μ the Green's function $G(\mathbf{k}, \omega)$ is needed, and for the determination of $G(\mathbf{k}, \omega)$ one has to know μ . This cycle can be avoided by as follows. One can infer the chemical potential directly from the energies of the excited states obtained by the ED. An approximate value for the chemical potential is then given by

$$\mu_{\text{ED}} = \frac{E_{\text{min}}^{\text{IPES}} + E_{\text{max}}^{\text{PES}}}{2}, \quad (11)$$

with $E_{\text{min}}^{\text{IPES}}$ the minimal energy of inverse-photo-emission (IPES) states and $E_{\text{max}}^{\text{PES}}$ the maximum energy of photo-emission (PES) states. This value only weakly depends on the mean-field and variational parameters, and as discussed below we found in all our calculations a well established gap between the PES and IPES states yielding a constant density n in a reasonably large neighborhood of the physical chemical potential μ , in agreement with quantum Monte Carlo calculations.³⁵ Therefore μ_{ED} gives a reasonable approximation for our calculations.

For the details of this method and the calculation of the grand potential we refer the reader to Refs. 30,31,33,34 and references therein.

III. RESULTS FOR SINGLE LADDERS

A. Critical coupling

We start our investigations with decoupled ladders, i.e., $t_{xy} = 0$ and $V_{xy} = 0$ (Fig. 1). Before we turn to the spectral function, we study the charge-ordering transition as a function of V . Since we will apply a mean-field decoupling of the nonlocal Coulomb interactions across cluster boundaries as described in Sec. II, we first study the effect of this approximation. For this purpose we consider the EHM without coupling to the lattice in the limit of exactly one electron per rung and $t_b = 0$. In mean-field approximation this case results in a second-order phase transition between a disordered state and a zig-zag ordered state at a critical interaction of $V_c^{\text{MF}} = 1.0$. On the other hand this case is exactly solvable by a mapping to an Ising model in a transverse field,²² yielding a critical interaction of $V_c^{\text{exact}} = 2.0$.³⁶ Thus we expect strong mean-field effects, since in this special limit we found $V_c^{\text{exact}} = 2V_c^{\text{MF}}$. Since it can be assumed that a finite value of the hopping between adjacent rungs t_b weakens the charge ordering, the actual critical value V_c is presumably located slightly above 2.0 when t_b is included.

In order to determine the order of the transition within the framework of V-CPT it is sufficient to calculate the grand potential Ω , Eq. (7), as a function of the mean-field parameters.³⁴ Since our system is quarter filled we

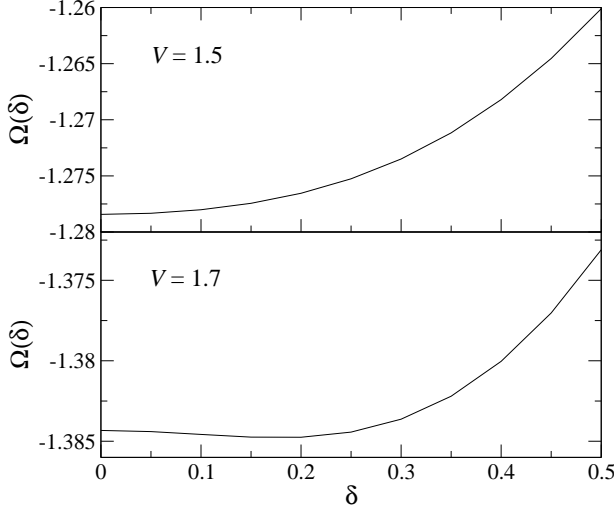


FIG. 2: Grand potential $\Omega(\delta)$ as a function of the mean-field parameter δ with a 6×2 cluster serving as reference system, and without coupling to the lattice. Upper panel: $V = 1.5$. Lower panel: $V = 1.7$.

consider only one parameter δ giving mean-field electron densities $\langle n \rangle + \delta$ and $\langle n \rangle - \delta$ on sublattices A and B , respectively. For second-order phase transitions it can in addition be important to include a fictitious staggered chemical potential as a variational parameter.³⁴ This field is included via the single-particle operator $\mathcal{O}(\mathbf{R})$, Eq. (6), with

$$\Delta_{a,b} = \varepsilon \delta_{a,b} e^{i\mathbf{Q}\mathbf{r}_a}, \quad (12)$$

where ε denotes the variational parameter, \mathbf{r}_a is the lattice vector of site a , and $\mathbf{Q} = (\pi, \pi)$. Initial calculations showed that in the present case the inclusion of such a field does not have any significant effect and the relative change in Ω is at most of the order of 10^{-4} . For this reason all further calculations have been done without a staggered chemical potential.

Fig. 2 shows the dependence of $\Omega(\delta)$ on the mean-field parameter δ calculated with a 6×2 cluster as reference system. For simplicity we set $V_a = V_b = V$. One can see that the system undergoes a continuous phase transition,³⁴ which is located between $V = 1.5$ and $V = 1.7$. This value for the critical interaction is considerably smaller than the above mentioned value of the analytical solution, but the agreement is much better than the result of the purely mean-field calculation, $V_c^{\text{MF}} = 1.0$.

In order to study the finite-size dependence of the critical Coulomb interaction we performed calculations on clusters of different length, and the results are depicted in Fig. 3. The steps in V in our calculations were $\Delta V = 0.01$, which results in error bars of $\Delta V_c = 0.005$. As expected, V_c is strongly finite-size dependent. From Fig. 3 we can expect that for larger cluster sizes the critical interaction V_c increases further and reaches the expected value of slightly above 2.0, but for a more sophis-

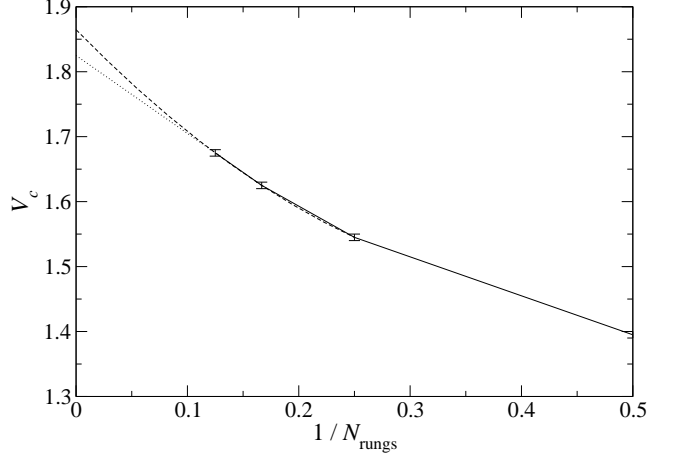


FIG. 3: Finite-size dependence of the critical Coulomb interaction V_c without lattice coupling. Error bars are due to the finite step $\Delta V = 0.01$ in the calculations. Dotted line: Linear extrapolation of the 8 and 6 rung cluster. Dashed line: Quadratic extrapolation of the 8, 6, and 4 rung cluster.

ticated finite-size scaling our cluster sizes are too small. Nevertheless it is possible to study the spectral function both in the disordered and the ordered phase. Since the calculations for the 8×2 ladder are very time consuming, all single-ladder spectra presented in this paper have been determined with a 6×2 ladder as reference system.

B. Disordered phase

We start our investigations of the spectral function with the disordered high-temperature phase. Since α' -NaV₂O₅ may be near a quantum critical point between ordered and disordered phase, we choose the nearest neighbor interaction to be slightly below the critical value. We set $V = V_a = V_b = 1.3$, $t_b = 0.5$, and we do not include diagonal hopping, i.e. $t_d = 0$. The result of this calculation is shown in Fig. 4. An additional Lorentzian broadening of $\eta = 0.1$ has been used for all spectra shown in this paper. The dashed vertical line marks μ_{ED} calculated from Eq. (11), and the dotted line denotes μ_{CPT} determined from the condition Eq. (9). For the latter quantity the sum over momentum vectors had to consist of about 80 vectors in order to get a well converged result. It is easy to see that $\mu_{\text{ED}} = 1.71$ lies exactly in the middle of the gap, whereas $\mu_{\text{CPT}} = 1.23$ is located at its lower boundary. But since there are no in-gap states both values of μ give approximately the same average density n , and the ground-state energy $E_0 = \Omega + \mu N$ hardly depends on whether we use μ_{ED} or μ_{CPT} . These facts confirm that our approximation to use $\mu = \mu_{\text{ED}}$ as chemical potential gives correct results, and in addition the numerical effort for this procedure is much less than for the above described self-consistent determination of μ .

As one can easily see in Fig. 4, the spectral function

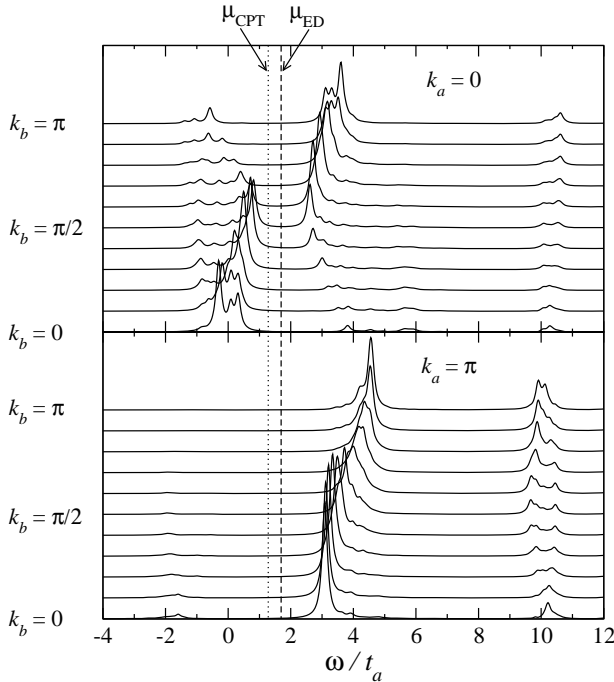


FIG. 4: Single-particle spectral function $A(\mathbf{k}, \omega)$ calculated with a 6×2 cluster in the disordered phase at $V_a = V_b = 1.3$. Top panel: Momentum $k_a = 0$ perpendicular to the ladder. Bottom panel: $k_a = \pi$. The dashed line marks the chemical potential calculated by Eq. (11), the dotted line marks the result obtained from Eq. (9).

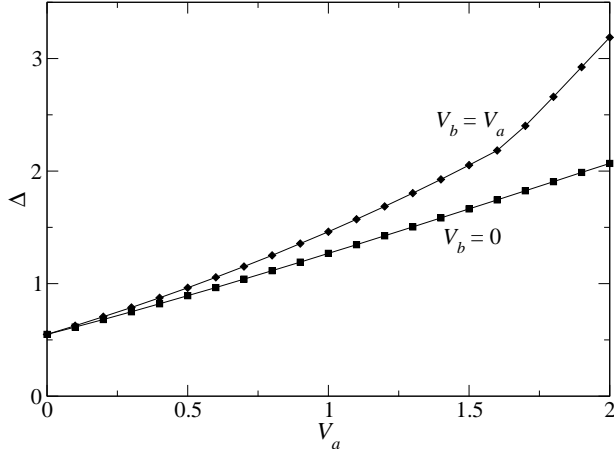


FIG. 5: Gap Δ in the spectral function as a function of V_a . Squares: $V_b = 0$. Diamonds: $V_b = V_a$.

exhibits a well defined gap around the chemical potential, a clear indication of insulating behavior. In order to check if the insulator is only stable above some critical inter-site Coulomb interaction, we calculated the gap Δ at $(k_a, k_b) = (0, \pi/2)$ as a function of the intra-rung interaction V_a . We studied two cases with $V_b = 0$ and $V_b = V_a$, respectively, and the results are shown in Fig. 5. Note that for $V_b = 0$ no mean-field decoupling is needed, since there are no interaction bonds between different

clusters. At $V_a = 0$, where both cases are equivalent, we found a finite value of the gap, $\Delta \approx 0.55$. We checked the finite size dependence by calculating the gap on a 4×2 cluster giving $\Delta \approx 0.59$. By applying a linear $1/N_{\text{rungs}}$ extrapolation to $N_{\text{rungs}} = \infty$ one gets $\Delta \approx 0.47$, indicating that the curves in Fig. 5 somewhat overestimates the value of the gap for the infinite ladder. Nevertheless we conclude from our calculations that the system is insulating already for small values of V_a . This is consistent with DMRG calculations,²⁷ where for $t_a > t_b$ a homogeneous insulating phase has been found for $V = 0$. The behavior of the spectral function is also in agreement with ED calculations on small clusters for $V = 0$, where for large enough t_a an insulating state has been found.²⁶ Similar results have been obtained by Kohno³⁷ for the $U = \infty$ Hubbard ladder.

In the case $V_b = 0$, which means that there is no Coulomb interaction between adjacent rungs, we found that Δ increases linearly with V_a . For $V_b = V_a$ the gap is slightly larger and the deviation increases with increasing V_a . Here, with a 6×2 cluster as reference system, the system starts to order at $V_c \approx 1.625$, which results in the kink in Δ around this critical value. Note that for $V_b = 0$ such a phase transition is not possible.

Let us now discuss the spectral features for $k_a = 0$ as shown in Fig. 4. The spectral function looks very similar to that of the half-filled one-dimensional Hubbard model with a totally filled lower and an empty upper band. Different from the 1D Hubbard model the gap between these two bands is not only determined by the onsite interaction U , but mainly by the intrarung interaction V_a , as discussed above. At $\mathbf{k} = (0, 0)$ one can see signatures of spin-charge separation, where the band is split into a low energy spinon band (at approximately $\omega - \mu \approx -1.5$) and a holon band at slightly higher energy ($\omega - \mu \approx -2.0$). This splitting has not been seen directly in experiments,^{11,12} since it is small and temperature effects did not allow a high enough experimental resolution. However, by studying the temperature dependence of ARPES spectra, it was argued that subtle spectral-weight redistributions can be related to spin-charge separation.¹³ Some spectral weight can also be found at very high energies of about $(\omega - \mu) \approx 8.5$, which is close to the onsite energy $U = 8$ and can thus be related to doubly-occupied sites.

Infrared (IR) experiments probe transitions near the Γ point, that is between even $(0, 0)$ and odd $(0, \pi)$ states in the language of single ladders. From Fig. 4 one can extract an excitation energy of roughly $3t_a$, which is in good agreement with the experimentally found 1 eV absorption.³⁸

The lower and upper band disperse with period π indicating a doubling of the unit cell in real space, similar to the 1D Hubbard model. In order to determine the origin of this doubling we have calculated the real-space spin correlation function $S_r = \langle S_1^z S_{1+r}^z \rangle$ within the cluster by exact diagonalisation, where S_1^z and S_r^z are the z -components of a spin on the cluster boundary and

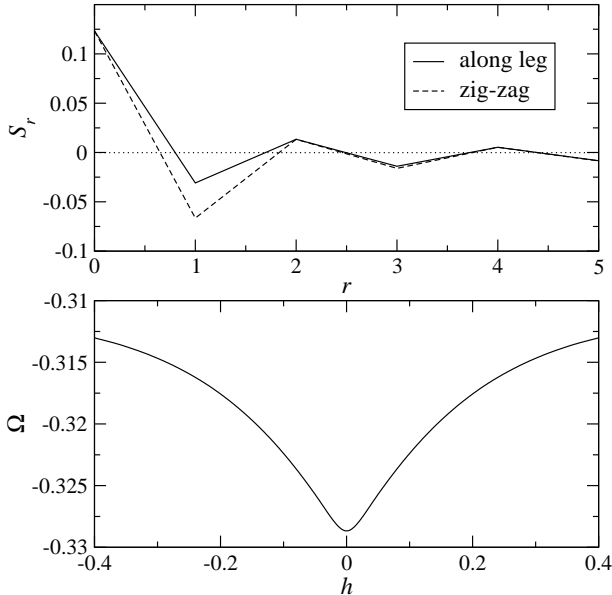


FIG. 6: Magnetic properties of a single ladder at $V_a = V_b = 1.3$. Upper panel: Spin correlation function $S_r = \langle S_1^z S_{1+r}^z \rangle$ calculated on an isolated 6×2 cluster. Lower panel: Grand potential Ω as a function of the strength of the fictitious field Eq. (13).

on a rung with distance r to the boundary. In the upper panel of Fig. 6 this correlation function is shown for two different paths, where the solid line is S_r along one leg of the ladder, and the dashed line is S_r on a zig-zag path through the ladder. Both correlation functions show clear antiferromagnetic correlations along the ladder similar to results obtained by the finite-temperature Lanczos method.²⁵ By applying a fictitious symmetry-breaking magnetic field via the operator $\mathcal{O}(\mathbf{R})$, Eq. (6), we can estimate whether this ordering is of long-range type or not. Similar to Ref. 33 we choose for this field

$$\Delta_{a,b} = h \delta_{a,b} z_\sigma e^{i \tilde{Q} \mathbf{r}_a}, \quad (13)$$

where z_σ is ± 1 for spin \uparrow, \downarrow in the orbitals a, b , and h is the field strength. The wave vector \tilde{Q} is set to $(0, \pi)$ yielding a staggered field along the ladder. The dependence of Ω on this fictitious field is depicted in the lower panel of Fig. 6. Similar to the one-dimensional Hubbard model at half filling,³³ there is only one stationary point at $h = 0$, which means that the system does not show long-range antiferromagnetic order, but is rather in a paramagnetic state with short-range antiferromagnetic correlations.

The above considerations show that the system exhibits short-range antiferromagnetic spin correlations along the ladder, which can produce the doubled unit cell. Nevertheless it is also possible that the doubling of the unit cell is due to short-range charge correlations and not due to spin correlations. In order to clarify this point we calculated the spectral function at $V_b = 0$ and finite V_a , where no charge ordering is possible. Also in this case the periodicity of the bands with largest spec-

tral weight is π at $k_a = 0$ and 2π at $k_a = \pi$. This shows that below the phase transition at $V_a = 1.3$, the doubling of the unit cell is mainly due to short-range spin correlations, and charge correlations play only a minor role in this context.

When turning to $k_a = \pi$, the spectral function looks totally different. As one can easily see in Fig. 4 there is hardly any spectral weight below the chemical potential, which means that there are no occupied states in the channel $k_a = \pi$. This can be understood, because $k_a = \pi$ corresponds to an antibonding state within a rung, which has energy $2t_a$ relative to the bonding orbital and is therefore not populated in the ground state.

An obvious difference between the spectra for $k_a = 0$ and $k_a = \pi$ is that in the latter case the excitations with largest spectral weight located between $\omega \approx 3$ and $\omega \approx 4.5$ disperse with periodicity 2π instead of π . Qualitatively this can be understood as follows. When inserting a particle with $k_a = 0$, this electron will occupy a state in the bonding orbital. Since one of the two states in this orbital is already occupied, the additional particle must have opposite spin, and thus this particle is connected to the antiferromagnetic background. A particle with $k_a = \pi$ occupies a state in the antibonding orbital, and since this orbital is not occupied, both spin directions possess equal possibility. Therefore an electron with $k_a = \pi$ is not influenced by the antiferromagnetism in the ground state.

C. Disordered phase including diagonal hopping

So far we have studied single ladders only with hopping parameters t_a and t_b and neglected additional diagonal hopping processes t_d , as indicated in Fig. 1. These hopping processes have been important in first-principle calculations in order to fit the LDA bands correctly.³⁹ Moreover t_d has been important in C-DMFT calculations in order to describe the insulating state in the disordered phase properly.²⁸ In this section we study the effect of t_d within the V-CPT framework.

In Fig. 7 the spectral function is shown for $V_a = V_b = 1.3$, $t_b = 0.25$ and $t_d = 0.25$, where the hopping parameters are chosen similar to Ref. 28. Whereas the spectrum at $k_a = 0$ is almost indistinguishable from Fig. 4, we see a big difference at $k_a = \pi$. There is still hardly any spectral weight below the Fermi energy, but the band with largest spectral weight above the Fermi level is now located at approximately $\omega - \mu \approx 2.0$ and can be regarded as dispersionless.

From a qualitative point of view this can be explained by the dispersion of non-interacting fermions on a two-leg ladder in the presence of diagonal hopping, which is given by

$$\varepsilon(\mathbf{k}) = -t_a \cos k_a - 2t_b \cos k_b - 2t_d \cos k_a \cos k_b, \quad (14)$$

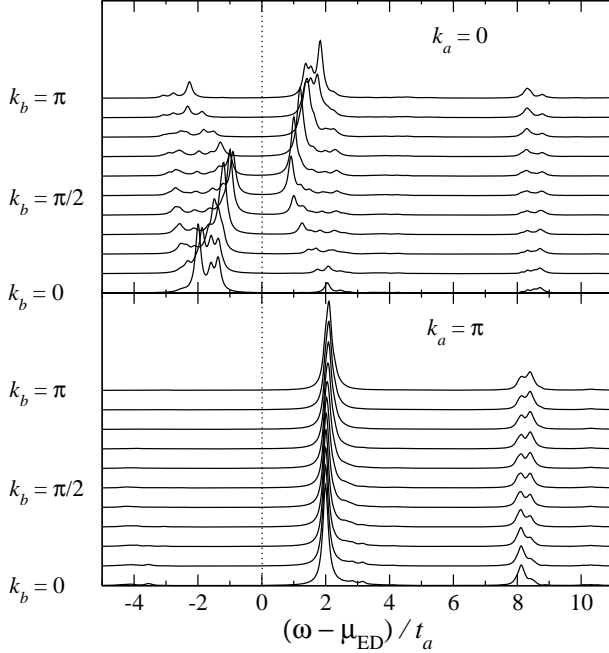


FIG. 7: Spectral function $A(\mathbf{k}, \omega)$ when the diagonal hopping is included, $t_b = 0.25$, $t_d = 0.25$. The Coulomb interaction was $V_a = V_b = 1.3$. The dotted line marks the chemical potential.

where the values for k_a are restricted to 0 and π , and in these two cases the dispersion can be written explicitly as

$$\varepsilon(k_a = 0, k_b) = -t_a - 2(t_b + t_d) \cos k_b \quad (15a)$$

$$\varepsilon(k_a = \pi, k_b) = +t_a - 2(t_b - t_d) \cos k_b. \quad (15b)$$

This means that for $k_a = 0$ the bandwidth is determined by the sum of t_b and t_d , whereas for $k_a = \pi$ it is set by the difference of these two hopping processes. Since we used $t_b = t_d = 0.25$, this fits perfectly to the spectrum shown in Fig. 7. The sum is equal to the value of t_b used for the calculations without diagonal hopping in Sec. III B, and the difference is equal to zero, which explains the dispersionless band at $k_a = \pi$.

The picture that evolves from our calculations is somewhat different to that obtained in first-principle and C-DMFT calculations. To begin with, the bands obtained from the LDA all disperse with periodicity 2π and not π , as observed experimentally, along the b direction. Moreover we could not find any signature of a flattening of the upper d_{xy} bands in the direction $\mathbf{k} = (0, 0) \rightarrow (0, \pi)$ when a diagonal hopping is included, which was reported in Ref. 39. The main difference of our calculations to C-DMFT results is that C-DMFT finds a metal-insulator transition at some finite value of V , and this transition point is shifted downward significantly when t_d is included.²⁸ In contrast we find an insulating state at reasonable values of U already for $V = 0$, even without the inclusion of t_d . The discrepancy to C-DMFT calculations are very likely due to the fact, that the cluster used in

the C-DMFT calculations consisted only of a single rung, and fluctuations along the ladders, which seem to be important in this system, have been neglected altogether.

D. Ordered phase

We investigate two different driving forces for the occurrence of a charge-order pattern, (i) the coupling of the electrons to lattice degrees of freedom, and (ii) nearest-neighbor Coulomb interaction, similar to Ref. 17.

Let us start our investigations with possibility (i), the coupling to the lattice. In order to keep the calculations simple, we consider static lattice distortions, as discussed in Sec. II. The inclusion of dynamical phonon effects would state a severe problem to the diagonalisation procedures, because for phonons the Hilbert space is a priori of infinite size, and some truncation scheme has to be applied.¹⁷ So far well converged results for the spectral function in the presence of dynamical phonons could only be achieved for the polaron and the bipolaron problem.⁴¹

We assumed a zig-zag charge order pattern, justified by experimental evidence:⁹

$$z_i = z e^{i \mathbf{Q} \cdot \mathbf{r}_i}. \quad (16)$$

In Ref. 17 the optimal value of z was determined by the minimum of the total energy. Here we minimize the SFA grand potential, Eq. (7). Thus the grand potential is now a function of two external parameters, the mean-field parameter δ and the static distortion z . In order to keep the calculations simple and the number of independent variables small, we did not consider an additional variational parameter like a staggered chemical potential.

Motivated by previous work,¹⁷ we set $V_a = V_b = 1.3$, since for this choice we expect the distortions to be close to the experimental value of $z_{\text{exp}} \approx 0.95$ (in units of 0.05 \AA). Indeed we found $z = 0.911$, which is close to z_{exp} , and the mean-field parameter was $\delta = 0.338$. The spectrum calculated with these values is shown in the top plots of Fig. 8.

The spectral function shows similar features as in the undistorted phase. For $k_a = 0$ the bands disperse with periodicity π , whereas for $k_a = \pi$ no evidence for a doubling of the unit cell can be found, and the periodicity is 2π . Nevertheless, the gap at $\mathbf{k} = (0, \pi/2)$ is considerably larger than for $V = 1.3$ without distortions, see Fig. 4.

An interesting quantity when considering charge-ordering phenomena is the charge order parameter, which we calculate as

$$m_{\text{CDW}} = \frac{1}{N_c \langle n \rangle} \sum_j (n_j - \langle n \rangle) e^{i \mathbf{Q} \cdot \mathbf{r}_j}. \quad (17)$$

The factor $\langle n \rangle$ in the denominator assures that the order parameter is normalized to the interval $[0, 1]$. For $V_a = V_b = 1.3$ and static distortions we obtained $m_{\text{CDW}} = 0.65$, which means that the disproportion of charges is rather large.

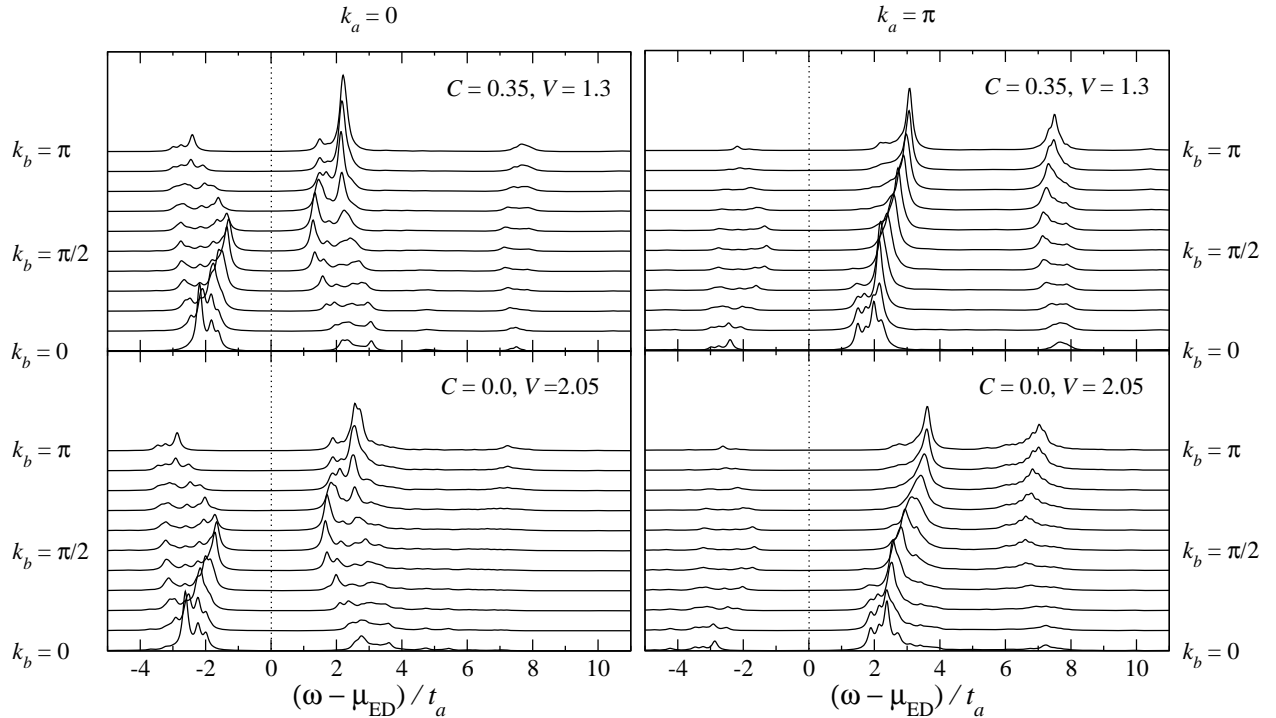


FIG. 8: Spectral function $A(\mathbf{k}, \omega)$ in the ordered phase. Top: Transition driven by coupling to the lattice. Bottom: Transition driven by Coulomb interaction. For the interaction $V = V_a = V_b$ was used, with the values as given in the plots. The dotted line marks the chemical potential.

Let us now consider possibility (ii), where the coupling to the lattice is switched off, $C = 0$, $\kappa = 0$, and the charge ordering is driven by the nearest-neighbor Coulomb interaction. In order to make a connection to the results obtained with lattice distortions, we calculate the spectral function at a similar value of the charge order parameter. We found that for $V_a = V_b = 2.05$ the order parameter is $m_{CDW} = 0.66$, close to the value found above.

The spectral function is shown in the lower plots of Fig. 8. The spectral features again look very similar to Fig. 4. By comparing the upper and lower plots of Fig. 8, one can see that in both cases the gap at $\mathbf{k} = (0, \pi/2)$ is larger than in the disordered phase, Fig. 4. To be specific we found a gap size of approximately $2.6t_a$ in the presence of lattice distortions and $3.4t_a$ without lattice distortions, whereas in the disordered phase the gap was $1.8t_a$. It is interesting that the momentum-resolved single-particle spectral features do depend on the driving force of the transition, which was much less pronounced for, e.g., spin and charge susceptibilities obtained by integration over the electron states.¹⁷

The excitation energy near the Γ point, relevant for IR experiments, can be read off from Fig. 8 to be roughly $4t_a$ with lattice distortions and $5t_a$ without distortions. Although these excitation energies are not constant compared to the disordered phase, calculations including the lattice degrees of freedom give a better agreement to experimental IR absorption data,³⁸ which show neither a shift of the 1 eV peak nor the appearance of new peaks

related to electronic transitions.

IV. RESULTS FOR COUPLED LADDERS

So far we studied only single ladders and neglected the inter-ladder couplings, since they are frustrated and one might assume that they are only of minor importance. Nevertheless our approach allows us to include these inter-ladder couplings by choosing an appropriate cluster geometry, as indicated on the right hand side of Fig. 1. Note that it is necessary to use a 2×12 super-cluster which allows for a commensurate charge order pattern across the cluster boundaries. For details of the treatment of super-clusters we refer the reader to Ref. 34.

The parameter values for the intercluster coupling are chosen in the following way. First-principle calculations have shown that the effective hopping between different ladders is very small, so we set $t_{xy} = 0.1t_a$, and longer ranging hopping processes are neglected since the linear dimensions of the cluster are rather small. The values for the other parameters are the same as used for the calculations in Sec. III B.

In Fig. 9 the spectral function for $V_a = V_b = V_{xy} = 1.3$ is shown. For \mathbf{k} parallel to the b axis one can easily see that the spectrum looks very similar to the spectrum of a single ladder (upper panel of Fig. 4). The main difference between single and coupled ladders is that the chemical potential is much larger in the latter case ($\mu \approx 3.0$),

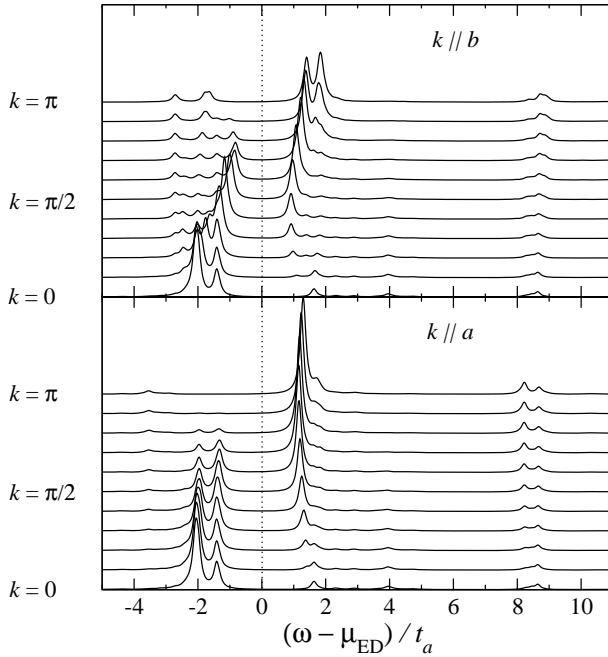


FIG. 9: Spectral function $A(\mathbf{k}, \omega)$ in the disordered phase at $V_a = V_b = V_{xy} = 1.3$ calculated on the 2×12 super-cluster. Top: Momentum k along the ladder direction. Bottom: k perpendicular to the ladder direction.

which is due to the frustrated inter-ladder bonds.

When turning to \mathbf{k} parallel to the a axis the spectral function looks very different. The most striking feature is that there is hardly any dispersion of the bands, and the filled low-energy band can actually be considered as dispersionless. The spectral weight of this excitation, however, decreases significantly away from $k = 0$ and is transferred to unoccupied states above the Fermi level at approximately $\omega - \mu \approx 1.5$.

Let us now compare our numerical results to experimental data. Kobayashi *et. al.*¹¹ performed angle-resolved photo-emission spectroscopy (ARPES) at room temperature, where the system is in the disordered phase. For momentum transfer parallel to the a direction they found no dispersion of the V 3d bands, which fits perfectly well to our results. For k along the b axis a band dispersion of a 1D antiferromagnetic quantum system was found with experimental band width of approximately 0.06–0.12 eV. This value is rather small compared to the band width in our calculation of approximately 0.35 eV, see Fig. 9. We checked that the band width scales with the hopping along the ladder t_b (not shown), and therefore this discrepancy between calculations and experiment can be shortened by choosing a smaller value for t_b , which does not significantly affect the charge ordering of the system. Nevertheless the strong difference between spectra along a and b direction are well described by our calculations.

V. CONCLUSIONS

In this paper we have applied the recently proposed generalization of the V-CPT for extended Hubbard models to the case of quarter-filled ladder compounds. We were thus able to perform the first theoretical study of the spectral function of α' -NaV₂O₅ within the extended Hubbard model.

For single ladders in the disordered phase we found that in the channel $k_a = 0$ the system behaves like a one-dimensional antiferromagnetic insulator, and the gap is mainly determined by the nearest-neighbor Coulomb interaction on a rung. Our calculations suggest that the system is in an insulating phase for all values of V .

This picture still holds when a diagonal hopping t_d is included in the Hamiltonian, which was suggested to be important by LDA and C-DMFT studies. We could show that for $k_a = 0$ hardly any changes can be seen in the spectral function, whereas for $k_a = \pi$ the bands become flat. These findings do not agree with LDA considerations,³⁹ where a flat upper band was observed for $k_a = 0$, thus requiring a finite value of t_d in a tight-binding fit.

For the transition into the charge-ordered low-temperature phase we considered two driving mechanisms, the coupling to a static lattice distortion and the nearest neighbor Coulomb interaction. With lattice coupling we found, similar to Ref. 17, that for $V = 1.3$ the distortion is close to the experimentally found size, accompanied by a large disproportion of charges. In order to reach the charge-ordered phase solely by Coulomb interactions, we had to use a large value of V (with $V = 2.05$ for the same value of the order parameter), which resulted in a large gap in the spectral function, considerably larger than in the disordered phase and in the ordered phase with lattice distortions. Since IR experiments³⁸ do not show such a discrepancy, we suggest that for the description of the ordered phase, lattice distortions cannot be neglected.

Within our approach it was straightforward to study the effects of inter-ladder coupling on the spectral function. We found that the spectra along the ladder direction are not significantly affected by these couplings. Perpendicular to the ladders the calculated bands are almost dispersionless, in good agreement with experimental data.

Acknowledgments

This work has been supported by the Austrian Science Fund (FWF), project P15520. M. A. has been supported by a doctoral scholarship program of the Austrian Academy of Sciences. We are grateful to E. Arrigoni and A. Damascelli for interesting discussions.

¹ A. Carpy and J. Galy, *Acta Crystallogr., Sect. B: Struct. Crystallogr. Cryst. Chem.* **31**, 1481 (1975).

² M. Isobe and Y. Ueda, *J. Phys. Soc. Jap.* **65**, 1178 (1996).

³ M.N. Popova, A.B. Sushkov, S.A. Klimin, E.P. Chukalina, B.Z. Malkin, M. Isobe, and Y. Ueda *Phys. Rev. B* **65**, 144303 (2002).

⁴ H.G. Schnering, Yu. Grin, M. Kaupp, M. Somer, R.K. Kremer, O. Jepsen, T. Chatterji, and M. Weiden, *Z. Kristallogr.* **213**, 246 (1998).

⁵ H. Smolinski, C. Gros, W. Weber, U. Peuchert, G. Roth, M. Weiden, and C. Geibel, *Phys. Rev. Lett.* **80**, 5164 (1998).

⁶ A. Meetsma, J.L. de Boer, A. Damascelli, J. Jegoudez, A. Revcolevschi, and T.T.M. Palstra, *Acta Crystallogr., Sect. C: Cryst. Struct. Commun.* **54**, 1558 (1998).

⁷ T. Ohama, H. Yasuoka, M. Isobe, and Y. Ueda, *Phys. Rev. B* **59**, 3299 (1999).

⁸ E.Ya. Sherman, M. Fischer, P. Lemmens, P.H.M. van Loosdrecht, and G. Güntherodt, *Europhys. Lett.* **48**, 648 (1999).

⁹ J. Lüdecke, A. Jobst, S. van Smaalen, E. Morre, C. Geibel, and H.-G. Krane, *Phys. Rev. Lett.* **82**, 3633 (1999).

¹⁰ P. Horsch and F. Mack, *Eur. Phys. J. B* **5**, 367 (1998).

¹¹ K. Kobayashi, T. Mizokawa, A. Fujimori, M. Isobe, and Y. Ueda, *Phys. Rev. Lett.* **80**, 3121 (1998).

¹² A. Damascelli, private communication.

¹³ K. Kobayashi, T. Mizokawa, A. Fujimori, M. Isobe, Y. Ueda, T. Tohyama, and S. Maekawa, *Phys. Rev. Lett.* **82**, 803 (1999).

¹⁴ J. Riera and A. Poilblanc, *Phys. Rev. B* **59**, 2667, (1999).

¹⁵ R.T. Clay and S. Mazumdar, cond-mat/0305479.

¹⁶ E.Ya. Sherman, C. Ambrosch-Draxl, P. Lemmens, G. Güntherodt, and P.H.M. van Loosdrecht, *Phys. Rev. B* **63**, 224305 (2001).

¹⁷ M. Aichhorn, M. Hohenadler, E.Ya. Sherman, J. Spitaler, C. Ambrosch-Draxl, and H.G. Evertz, *Phys. Rev. B* **69**, 245108 (2004).

¹⁸ M. Fischer, P. Lemmens, G. Els, G. Güntherodt, E.Ya. Sherman, E. Morre, C. Geibel, and F. Steglich, *Phys. Rev. B* **60**, 7284 (1999).

¹⁹ J. Spitaler, E.Ya. Sherman, C. Ambrosch-Draxl, and H.G. Evertz, *Physica Scripta* **T109**, 159 (2004); *Phys. Rev. B*, in print.

²⁰ H. Seo and H. Fukuyama, *J. Phys. Soc. Jpn.* **67**, 2602 (1998).

²¹ P. Thalmeier and P. Fulde, *Europhys. Lett.* **44**, 242 (1998).

²² M. Mostovoy and D.I. Khomskii, *Solid State Commun.* **113**, 159 (2000); M.V. Mostovoy, D.I. Khomskii, and J. Knoester, *Phys. Rev. B* **65**, 064412 (2002).

²³ M. Cuoco, P. Horsch, and F. Mack, *Phys. Rev. B* **60**, R8438 (1999).

²⁴ A. Hübsch, C. Waidacher, K.W. Becker, and W. von der Linden, *Phys. Rev. B* **64**, 075107 (2001).

²⁵ M. Aichhorn, P. Horsch, W. von der Linden, and M. Cuoco *Phys. Rev. B* **65**, 201101(R) (2002).

²⁶ J. Riera, D. Poilblanc, and E. Dagotto, *Eur. Phys. J. B* **7**, 53 (1999).

²⁷ M. Vojta, A. Hübsch, and R.M. Noack, *Phys. Rev. B* **63**, 045105 (2001); M. Vojta, R.E. Hetzel, and R.M. Noack, *Phys. Rev. B* **60**, R8417 (1999); R. M. Noack, S.R. White, and D.J. Scalapino, *Physica C* **270**, 281 (1996).

²⁸ V.V. Mazurenko, A.I. Lichtenstein, M.I. Katsnelson, I. Dasgupta, T. Saha-Dasgupta, and V.I. Anisimov, *Phys. Rev. B* **66**, 081104 (2002).

²⁹ E. Orignac and R. Citro, *Eur. Phys. J. B* **33**, 419 (2003).

³⁰ M. Potthoff, M. Aichhorn, and C. Dahnken, *Phys. Rev. Lett.* **91**, 206402 (2003).

³¹ C. Gros and R. Valenti, *Phys. Rev. B* **48**, 418 (1993), D. Sénéchal, D. Pérez, and M. Pioro-Ladrière, *Phys. Rev. Lett.* **84**, 522 (2000); D. Sénéchal, D. Pérez, and D. Plouffe, *Phys. Rev. B* **66**, 075129 (2002).

³² M. Potthoff, *Eur. Phys. J. B* **32**, 429 (2003), *Eur. Phys. J. B* **36**, 335 (2003).

³³ C. Dahnken, M. Aichhorn, W. Hanke, E. Arrigoni, and M. Potthoff, cond-mat/0309407 (Phys. Rev. B, in print).

³⁴ M. Aichhorn, H.G. Evertz, W. von der Linden, and M. Potthoff, cond-mat/0402580.

³⁵ C. Gabriel, E. Sherman, T.C. Lang, M. Aichhorn, and H.G. Evertz, cond-mat/0406715.

³⁶ E. Lieb, T. Schultz, and D. Mattis, *Ann. Phys. (N.Y.)* **16**, 407 (1961); T.H. Niemeijer, *Physica (Amsterdam)* **36**, 377 (1967); P. Pfeuty, *Ann. Phys. (N.Y.)* **57**, 79 (1970).

³⁷ M. Kohno, *Phys. Rev. B* **56**, 15015 (1997).

³⁸ A. Damascelli, D. van der Marel, M. Grüninger, C. Presura, T.T.M. Palstra, J. Jegoudez and A. Revcolevschi, *Phys. Rev. Lett.* **81**, 918 (1998); C. Presura, D. van der Marel, A. Damascelli, and R.K. Kremer, *Phys. Rev. B* **61**, 15762 (2000).

³⁹ A.N. Yaresko, V.N. Antonov, H. Eschrig, P. Thalmeier, and P. Fulde, *Phys. Rev. B* **62**, 15538 (2000).

⁴⁰ M. Aichhorn, M. Daghofer, H.G. Evertz, and W. von der Linden, *Phys. Rev. B* **67**, 161103(R) (2003).

⁴¹ M. Hohenadler, M. Aichhorn, and W. von der Linden, *Phys. Rev. B* **68**, 184304 (2003) and cond-mat/0405391.